Creating an eco-friendly building coating with smart sub-ambient radiative cooling

Xiao Xue[1,2*], Meng Qiu[3*], Yanwen Li[1,4], Q. M. Zhang[5], Siqi Li[6], Zhuo Yang[2], Chi Feng[1], Weidong Zhang[1,†], Jian-Guo Dai[2,†], Dangyuan Lei[7,6,†,‡], Wei Jin[3], Lijin Xu[4], Tao Zhang[1], Jie Qin[1], Huiqun Wang[1,8], Shanhui Fan[9]

[1]Technical Center, China State Construction Engineering Co., Ltd., Beijing 101300, China.
[2]Department of Civil and Environmental Engineering, The Hong Kong Polytechnic University, Hung Hom, Hong Kong, China
[3]Department of Electrical Engineering, The Hong Kong Polytechnic University, Hung Hom, Hong Kong, China
[4]Department of Chemistry, Renmin University of China, Beijing 100872, China
[5]School of Electrical Engineering and Computer Science, Pennsylvania State University, University Park, PA 16802, USA
[6]Department of Applied Physics, The Hong Kong Polytechnic University, Hung Hom, Hong Kong, China
[7]Department of Materials Science and Engineering, City University of Hong Kong, 83 Tat Chee Avenue, Kowloon, Hong Kong, China
[8]Harbin Zhongke Materials Engineering Co., Ltd., Harbin 150050, China
[9]Center for Nanoscale Science and Engineering, Stanford University, Stanford, CA 94305-4088, USA

***These authors contribute equally to this work.**

[†]Corresponding author. Email: zwdpt@sohu.com (W. D. Z); cejgdai@polyu.edu.hk (J. G. D); dangylei@cityu.edu.hk (D. Y. L).

[†]Lead contact. Email: dangylei@cityu.edu.hk (D. Y. L).

GRAPHICAL ABSTRACT

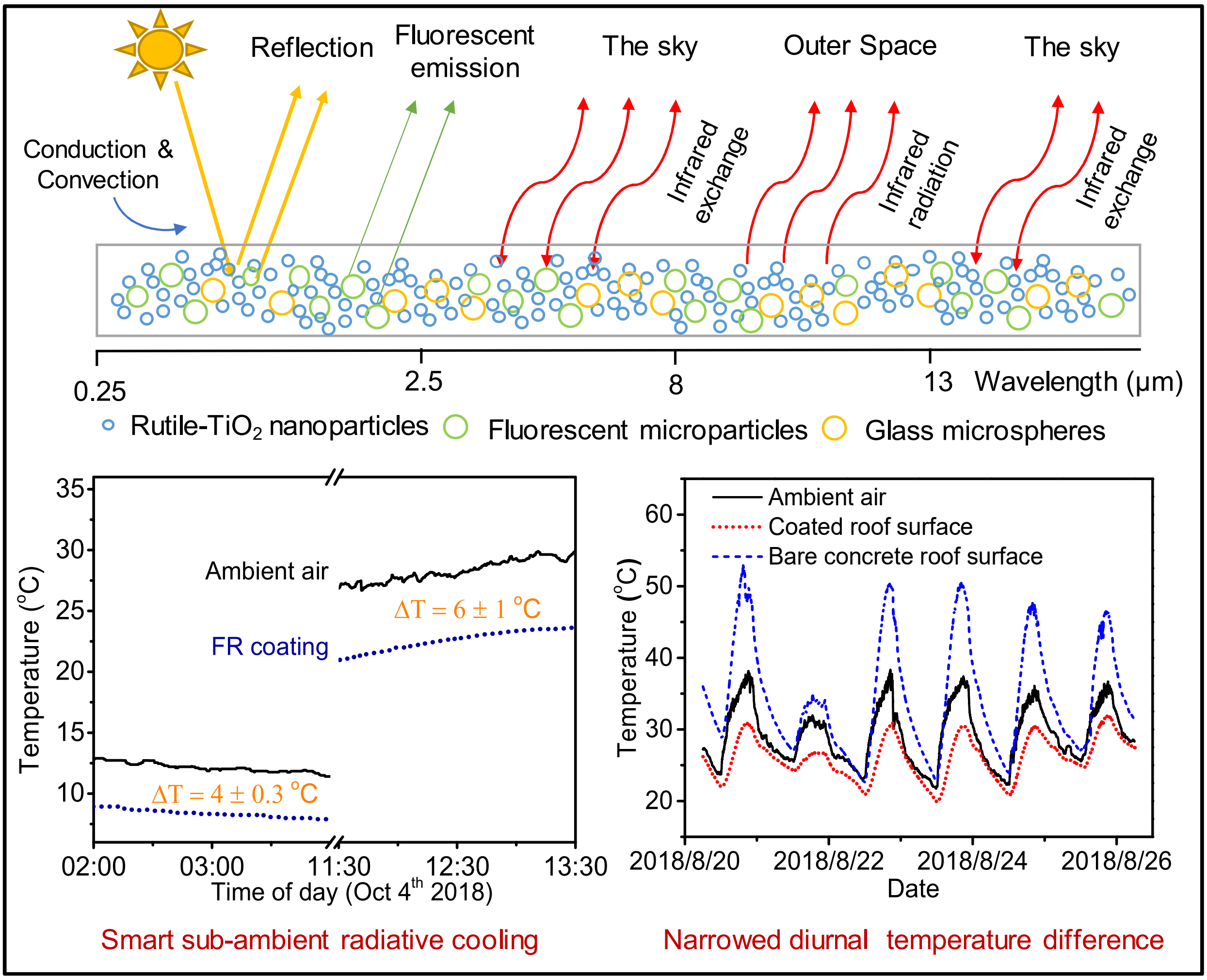

Conceptual illustration of fluorescence-enhanced smart sub-ambient radiative cooling (top) and cooling performance at the rooftop (lower-left) and over a scale-model building (lower-right)

HIGHLIGHTS:

- The all-construction-materials-made coating converts part of the solar absorption to fluorescence emission and thus improves its effective solar reflectance to realize sub-ambient daytime radiative cooling.
- The construction materials are formulated to possess simultaneously high reflectivity in the solar spectral region and enhanced broadband emissivity in the entire mid- and far-infrared region. Compared to the selective radiator utilizing solely the narrow atmospheric transparency window, the sky can be utilized as an additional cold source to enhance the cooling performance of the broadband radiator in daytime (6 °C reduction) while suppressing the cooling in nighttime (4 °C reduction).
- The SSRC coating achieves 7 °C cooling on a scale-model building during noon hours and also demonstrates peculiar eco-friendly and highly-scalable features and exceptional weather resistance.

Context & Scale

The active building cooling for keeping human thermal comfort is an energy-intensive activity, which is the biggest energy consumer in urban areas. Recently, sub-ambient daytime radiative cooling (SDRC) represents a breakthrough in the passive cooling technology, which minimizes the solar absorption and maximizes the heat dissipation into the outer space. Here, we propose a subtle design concept combining particle scattering, sunlight-excited fluorescence and mid-infrared broadband radiation, by which conventional building coating materials can be engineered at low cost to realize smart sub-ambient radiative cooling (SSRC). We demonstrate the wide applicability of our all-constructional-materials-based eco-friendly SSRC coating through both the device and field building model tests. The study opens up an innovative cost-effective avenue for achieving electricity-free building cooling through the advanced SSRC coating technology.

SUMMARY: Sub-ambient daytime radiative cooling (SDRC) provides a promising electricity- and cryogen-free pathway for global energy-efficiency. However, current SDRC systems require stringent surface designs, which are neither cost-effective nor eco-friendly, to selectively emit thermal radiation to outer space and simultaneously maximize solar reflectance. Here, we develop a generic method to upgrade the conventional building coating materials with a peculiar self-adaptive SDRC effect through combining particle scattering, sunlight-excited fluorescence and mid-infrared broadband radiation. We also theoretically prove that heat exchange with the sky can eliminate the use of resonant microstructures and noble metal mirrors in conventional SDRC, and also leads to enhanced daytime cooling yet suppressed nighttime overcooling. When exposed to direct sunlight, our upgraded coating over an aluminium plate can achieve 6 °C (7 °C on a scale-model building) below the ambient temperature under a solar intensity of 744 Wm^{-2} (850 Wm^{-2}), yielding a cooling power of 64.5 Wm^{-2}. The results pave the way for practical large-scale applications of high-performance SDRC for human thermal comfort in buildings.

INTRODUCTION

Building cooling during hot weather, which provides human thermal comfort and improves health and productivity, is critically important to our society. The peak demands of building cooling in cities pose a great challenge to power grids and may cause power blackouts[1]. Moreover, the refrigerant gases used in air conditioners are one of the largest contributors to greenhouse gas emissions[2]. Passive cooling, e.g., cooling with no power input and without greenhouse gas emission, provides an attractive solution to alleviate the power demands as well as negative environmental impact of building cooling.

Recent theoretical and experimental demonstrations of sub-ambient daytime radiative cooling (SDRC) represent a breakthrough in realizing passive daytime cooling[3-21]. These radiative cooling materials exploit the infrared transparency window of the atmosphere, in the wavelength range of 8 – 13 μm, to directly transmit heat from an object at ambient temperature, through blackbody radiation, to the cold outer space which has a temperature of 3 K (-270 °C). This radiation effect, in fact, is what causes one to feel chilly when staying outside in summer nights. However, to generate sub-ambient daytime cooling under direct sunlight using the same effect, the materials must overcome the heating generated by the direct sunshine. In order to realize that, these daytime radiative cooling materials were designed, using various approaches, to reflect most of the sunlight such that the heat absorption from the sun is below the level of radiative cooling. Based on the above SDRC concept, very recently the fluid-mediated cooling system[16,20] has been explored for use in building industry. However, the designs and fabrications of these SDRC coatings often rely on the use of sophisticated photonic microstructures[10,12-14,16], noble metal mirrors[10-16,20], metamaterials[15,20], or hazardous chemical processes[18], greatly limiting their practical large-scale building cooling applications[22]. Additionally, the sub-ambient daytime cooling reported in these existing devices ranges from 2.1 to 6.0 °C under direct sunlight in different regions[10,11,19,21], and in general their nighttime cooling power is much stronger than the daytime one because of less heat input at night[12-14,16,20,21]. The stronger nighttime cooing of these designs may result in an overcooling effect in cold winter (especially for the night time) when cooling is no longer needed (or heating is needed instead to keep the indoor thermal comfort) .Finally, it will enlarge the diurnal temperature difference that may jeopardize the service life of building envelopes because of the enlarged temperature variation, which induces significant thermal stresses in the building structures[22].

One intriguing question facing the research community is that whether the commercially used building coating materials can be engineered to realize enhanced sub-ambient daytime cooling yet suppressed nighttime overcooling, i.e. a "smart" sub-ambient radiative cooling (SSRC) in an eco-friendly and cost-effective manner. Solar reflective cool roof coatings are the most widely used and effective materials for building cooling in hot climates[23-26]. Through many decades of development efforts, a broad range of commercial building coating materials are now available. These materials are convenient to use in construction at low cost, and exhibit excellent durability[24,26], which are actually the practical barriers of transitioning the current SDRC technology for building cooling applications[10-16,19,20]. However, conventional TiO_2-based cool roof coatings have a typical solar reflectance of approximately 85%[26], which is not sufficiently high to meet the stringent requirements of SDRC. Therefore, developing new physical concepts to engineer these conventional building coating materials represents a promising cost-effective pathway for achieving SSRC.

In this work, we report that commonly used building coating materials, e.g., TiO_2 rutile powder, polymer emulsion and glass microsphere[23,26], can be engineered at low cost to surprisingly generate enhanced daytime radiative cooling of 6 ºC (7 °C on a scale-model building) under direct sunlight of 735 W/m^2 (4 ºC at nighttime), yielding a daytime cooling power of 64.5 W/m^2. Our SDRC design is greatly different from the existing approaches in the literature. Even though the TiO_2 particles have a strong absorption in the ultra-violet region, through the addition of fluorescent materials, part of the absorbed solar energy is effectively converted to fluorescence emission to yield an improved effective solar reflectance *(ESR)*[27,28], thus reducing the overall solar absorption. Additionally, the conventional building coating materials are formulated to possess a broad emissivity spectrum in the entire mid-infrared region instead of using the narrow spectrum matching that of the atmospheric transparency window. Thus, the passive cooling materials can access an additional cold source, the sky, which enhances cooling in daytime yet suppresses the excessive cooling at nighttime, creating the aforementioned SSRC. In addition to expanding SRDC design paradigms, our results remove the major barriers of existing SDRC systems that impede the large-scale practical applications in buildings.

RESULTS

Theoretical analysis of SSRC design

In general, the fundamental thermal processes involved in a typical SDRC device at temperature *T* can be grouped into four sources, as expressed in Eq. (1) below:

$$P_{\text{cool}}(T) = P_{\text{rad}}(T) - P_{\text{sun}} - P_{\text{atm}} - P_{\text{cond+con}} \qquad (1)$$

where $P_{rad}(T)$, P_{sun} and P_{atm} are the thermal radiation, solar absorption and atmospheric longwave radiation absorbed by the device, respectively, and $P_{cond+conv}$ is the device's heat convection and conduction with the surrounding environment[10]. These items can be expressed as:

$$P_{\text{sun}} = \int A_{\text{RC}}(\lambda) I_{\text{sun}}(\lambda) \mathrm{d}\lambda \qquad (2)$$

$$P_{\mathrm{rad}} = \int A_{\mathrm{RC}}(\lambda) B(\lambda, T) \mathrm{d}\lambda \quad (3)$$

$$P_{\mathrm{atm}} = \int A_{\mathrm{RC}}(\lambda) DLR(\lambda) \mathrm{d}\lambda \quad (4)$$

where $A_{\mathrm{RC}}(\lambda)$ is the absorptivity spectrum of the device, I_{sun} is the solar spectrum, $B(\lambda, T)$ is the hemispherical black-body radiation power spectrum at T, $DLR(\lambda)$ is the atmospheric downward longwave radiation flux spectrum. In the existing SDRC designs in the literature, P_{sun} is minimized by designing materials and/or structures with high solar reflectance. In addition, due to the narrow emissivity spectrum of these designs, $P_{\mathrm{rad}}(T)$ and P_{atm} are limited to the atmospheric transparency window of 8 – 13 µm, beyond which the radiative heat exchange is strongly suppressed.

It is widely accepted that due to the limited radiation capacity, the steady-state temperature (when $P_{\mathrm{cool}}(T) = 0$) of the existing spectrum-selective SDRC designs is strongly affected by the parasitic thermal load. By extremely suppressing the parasitic heating of the environment (e.g. using a vacuum chamber), i.e., the convective coefficient h_c approaches zero, a spectrum-selective SDRC device was reported to be able to achieve a temperature reduction of 42 ºC[12]. With increasing h_c, which represents a more realistic working environment, however, the temperature reduction of the spectrum-selective SDRC design, with non-zero emissivity restricted to the wavelength range of 8 – 13 µm, may become inferior to that achieved by a broad spectrum SDRC design[12,13]. This is mainly because there are substantial non-zero transmission coefficients of the sky outside the main transparency window of 8 – 13 µm. For example, in addition to the main transparency window, we note that the downward radiation is also weak around the wavelength range of 20-25 microns as shown in Fig. S1 in the supplementary information. Hence an emitter with a broader bandwidth may provide additional cooling power to enhance the SDRC effect to offset the parasitic thermal load.

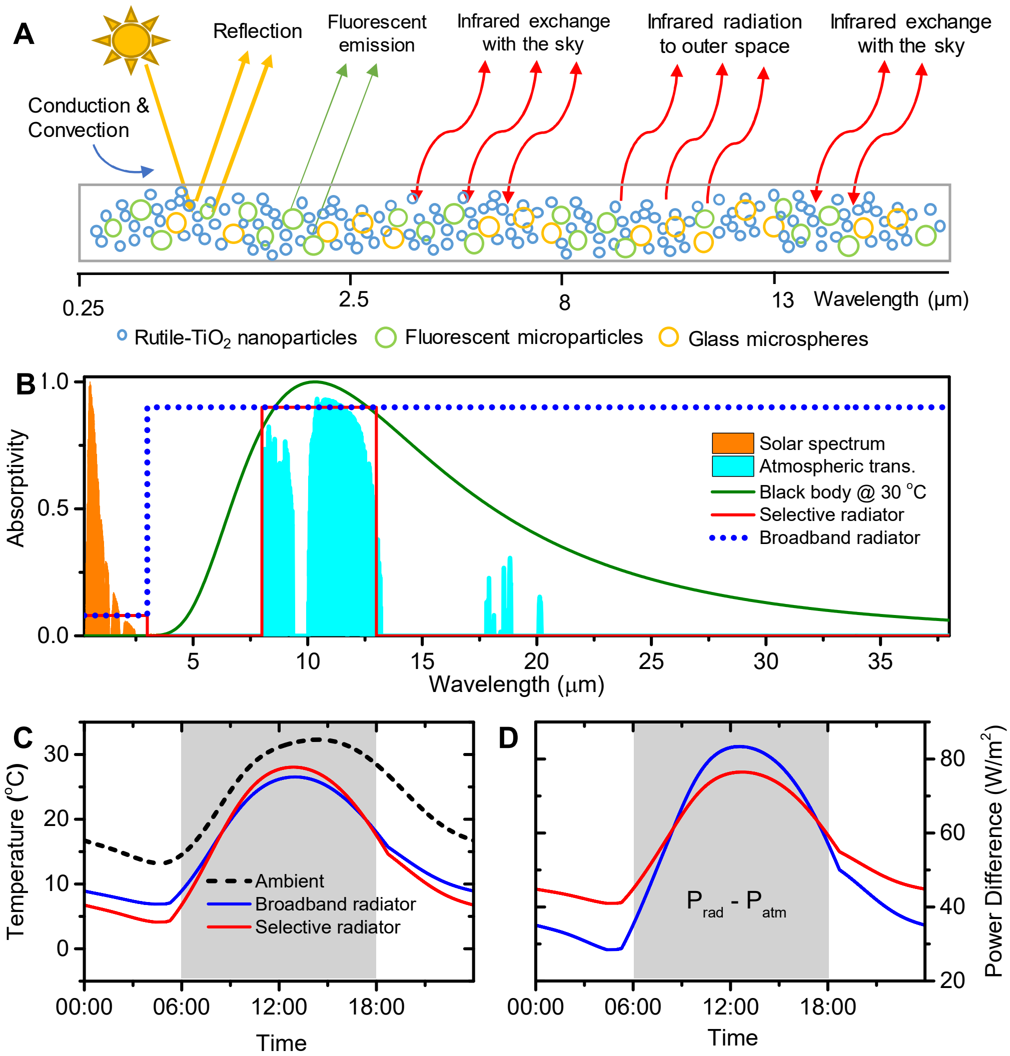

Figure 1. Theoretical analysis of smart sub-ambient radiative cooling. (A) Schematics of the cooling mechanism of the designed coating. (B) Standard solar spectrum, $I_{AM1.5}(\lambda)$ (orange), transmittance spectrum of the atmosphere, $t_{atm}(\lambda)$ (cyan), black-body radiation spectrum at 30 °C, $B(\lambda, 30\ °C)$ (green), ideal absorptivity spectra, $A_{RC}(\lambda)$ of a selective radiator (red) and a broadband radiator (blue). (C) Cooling temperatures calculated with Eq. (1) for the broadband radiator (blue) and the selective radiator (red), in comparison with the measured ambient temperature (black). (D) Calculated P_{rad} - P_{atm} for the broadband radiator (blue) and the selective radiator (red).

To quantify the effect of heat exchange with the sky (i.e. P_{rad} - P_{atm}) on the SDRC performance of the two types of radiators, we carry out theoretical calculations by assuming an ideal emissivity of 0.9 from 3 μm to 50 μm for the broadband radiator and the same emissivity from 8 μm to 13 μm for the selective radiator, respectively (see Figure 1B). To compare the SDRC performance of the two radiators under real working conditions, we set the solar absorptivity as 6.6% and h_c as 4.5 $Wm^{-2}K^{-1}$, respectively, as the experimentally achievable conditions. As a result of the above assumptions, the two radiators have the same P_{sun} but different P_{rad} - P_{atm}. Subsequently, we calculate the cooling temperatures of both radiators according to the measured meteorological data (i.e., solar intensity and DLR intensity, see Figure S1A) and the DLR flux spectrum (see Figure S1B) for a typical late summer sunny day in Beijing. As shown in Figure 1C, comparing with the ambient temperature (black dashed line), both radiators can achieve significant sub-ambient cooling during the entire day. However, the broadband radiator generates a cooling temperature to 26 °C at the noontime when cooling is needed, compared with 28 °C for the selective radiator. In the early morning (e.g., 2:00 a.m.) when cooling is no longer needed (e.g. the ambient air temperature is below 15 °C), the broadband and selective radiators generate cooling temperatures to 7 °C and 4 °C, respectively. The above comparison reveals an essential difference between the two types of radiators, that is, the broadband radiator enhances radiative cooling in daytime yet suppresses overcooling at nighttime, leading to a narrowed diurnal temperature difference compared to the selective one. Such a difference can be attributed to the broadband radiator's stronger heat exchange capacity with the sky. At noon, the sky is colder than the coatings; therefore, the open-sky model induces further cooling. Conversely, at night, the sky is warmer than the coatings; thus, the open-sky model suppresses overcooling. Figure 1D shows the variation of heat exchange with the sky for the two radiators during an entire day, indicating that the broadband radiator leads to a higher cooling power in daytime (e.g. 10:00 am – 4:00 pm) yet a lower cooling power at nighttime (e.g. 7:00 pm – 5:00 am). Note that we calculated P_{atm} using the measured DLR intensity and reported DLR flux spectrum.

Experimental realization of SSRC coating

To fabricate the designed SSRC coating working in the framework of the broadband radiator, we choose commercially available polystyrene-acrylates emulsion as the matrix material, and TiO_2 powder and glass microspheres as the functional fillers. Their constructability allows us to mix them easily to form a building coating (see Movie S1) and be conveniently applied on building envelops (see Movie S2).

Here TiO_2 is selected because of its high spectral reflectance in the visible (0.45 – 0.7 μm) and near infrared (0.7 – 2.5 μm) regions (see Fig. S2A). On the other hand, its absorptivity of the sunlight in the region (0.25 – 0.45 μm) results in an overall solar reflectance of less than 0.9 of a TiO_2-based coating, which is not high enough to reduce the direct sunlight heating and realize meaningful SDRC. To address this issue, a highly-efficient and low-cost fluorescent pigment ($SrAl_2O_4$:Eu^{2+},Dy^{3+},Yb^{3+}) is added to the polymer matrix as an additional filler to reduce the heat generated by the solar absorption through fluorescent emission. This strategy, as will be shown in the paper, removes the limitation of conventional coating materials in achieving very high solar reflectance. For the broadband emissivity needed for our broadband SSRC design, we purposely choose the above-mentioned three types of fillers with wide ranges of particle sizes (see Figure S3A-C). For the convenience of discussion, the coating with fluorescent pigment is termed "FR coating", while the control coating without fluorescent pigment yet specially designed following the broadband radiator (see its optical properties in the next section) is designated as "white coating" (see Supplemental Experimental Procedures S1 and S2).

Figure 2 shows the microstructures and optical properties of the FR and white coating samples (see measurement details in Supplemental Experimental Procedures S3-S6). As observed from the scanning electron microscopy (SEM) micrographs for the formed FR coating membrane in Figure 2A, the micro-sized fluorescent particles are uniformly mixed with the TiO_2 nanoparticles and glass microspheres. The emissivity spectra of each component and each combination of two components of the FR coating are presented in Figure S2B and C, all of which generally exhibit a broadband characteristic owing to multiple scatterings of broad-sized distributed inorganic particles in the polymer matrix. By combining them together, however, our coating with the three fillers exhibits an enhanced overall emissivity of approximately 0.90 between 3 to 50 μm and an even higher infrared emissivity of approximately 0.96 between 8 to 13 μm, indicating that strong emissivity exists both within and outside the atmospheric transparency window (Figure 2B).

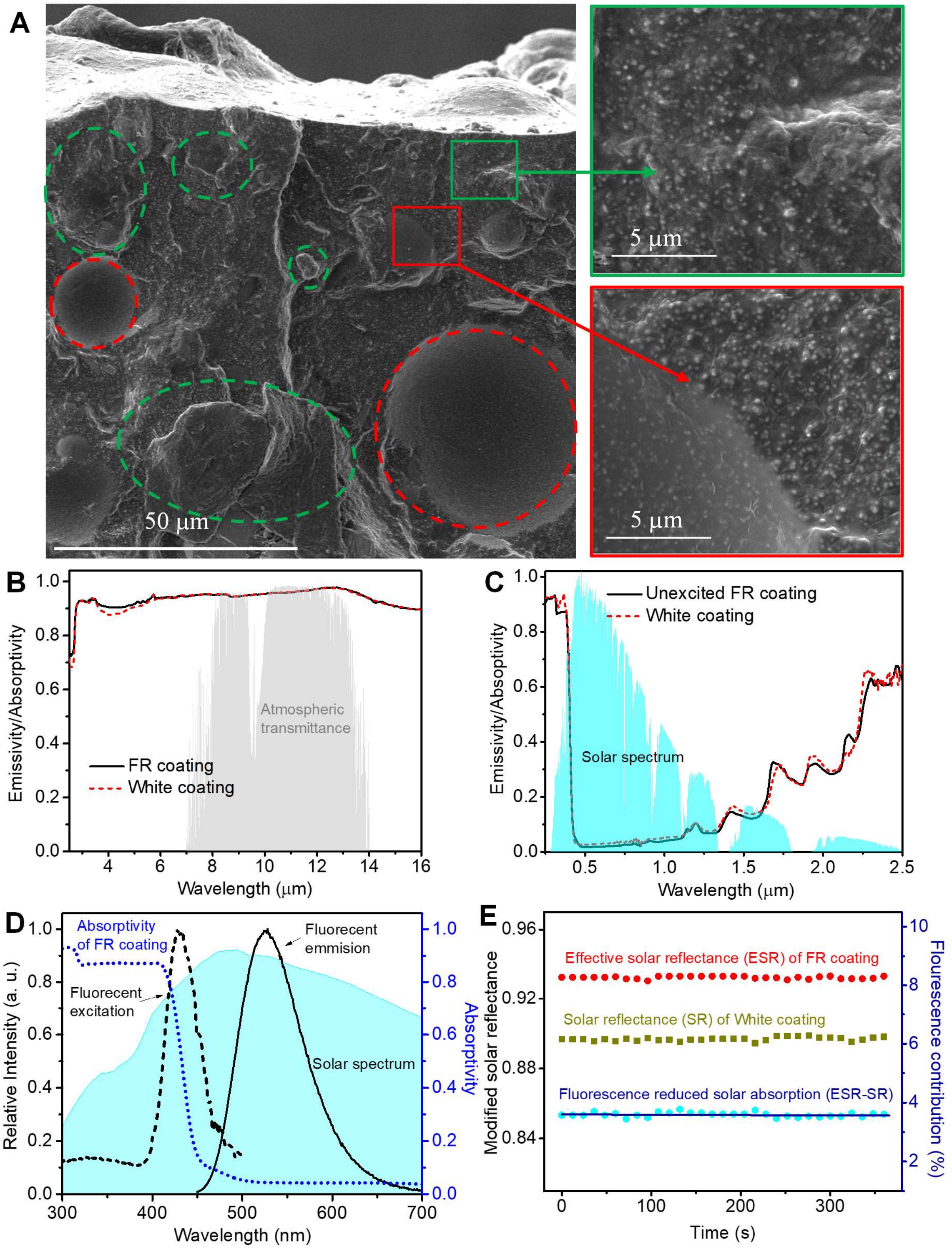

Figure 2. Microstructures and optical properties of FR and white coatings. (A) SEM micrographs of the FR coating. The left panel is a cross-sectional view image; the right two panels are enlarged view of a micro-sized fluorescent particle (green panel) and a hollow glass microsphere (red panel). Both images reveal uniform distribution of TiO_2 nanoparticles (white tiny particles). (B) Infrared emissivity spectra

and (C) solar absorptivity spectra of the FR coating (under unexcited state) and the white coating, overlaid with the atmospheric transmittance spectrum and the standard solar spectrum, respectively. (D) Absorption, fluorescent excitation and emission spectra of the FR coating, overlaid with the standard solar spectrum. (E) Modified ESR for the FR coating, the solar reflectance (SR) for the cool white coating and the extracted fluorescence-reduced solar absorption ($ESR - SR$ is equal to the generated fluorescent upflux).

Now we examine the absorption and fluorescence properties of the SSRC coating thus formed. The solar reflectance of the FR coating under the unexcited state and the white coating is 0.898 and 0.895, respectively (see Figure 2C and Table S1). Figure 2D shows that the excitation peak of the FR coating is around 420 nm, which is below the TiO_2 absorption band edge. It is obvious that the white and FR coatings should have almost the same solar reflectance under the unexcited state (Figure 2C). However, when exposed to the direct sunlight, the Purcell-effect-enhanced fluorescence emission[29,30] of the FR coating converts the sunlight around 420 nm to the 525 nm wavelength range (i.e., yellow-green luminescence) (Figure S4A, Figure 2D). Hence, the overall solar absorption in Eq. (1) is modified as:

$$P_{\text{sun}} = P_{\text{abs}} - P_{\text{fluo}} \quad (5)$$

where P_{abs} is the solar absorption of the coating, and P_{fluo} can be expressed as follows:

$$P_{\text{fluo}} = \alpha \beta_{\text{emit}} \Phi \int E_{\text{fluo}}(\lambda) A_{\text{RC}}(\lambda) I_{\text{sun}}(\lambda) d\lambda \quad (6)$$

where I_{sun} is the solar spectrum, $E_{\text{fluo}}(\lambda)$ is the excitation spectrum of the FR coating (black dashed line in Figure 2D), $A_{\text{RC}}(\lambda)$ is the absorptivity spectrum of the FR coating (blue dotted line in Figure 2D), and α is the proportion of P_{abs} for fluorescent excitation, β_{emit} is the ratio of fluorescence emission energy (black solid line in Figure 2D) and excitation energy, Φ is the fluorescence quantum yield of the FR coating.

In experiments, the power of fluorescence emission is integrated as $P_{\text{fluo}} = \eta P_{\text{sun}}$, in which $\eta = (ESR - SR)$ is measured using the setup shown in Figure S4B following ASTM E1918-16[31]. The ESR and SR are the measured upward radiative power of the FR coating and the white coating, respectively. The Purcell-effect-enhanced fluorescence emission compensates for the shortcoming of TiO_2's high absorption in the region of 0.25 – 0.45 µm. Consequently, the FR coating exhibits an ESR of 93.4% under direct sunlight (Figure 2E), which corresponds to an $ESR - SR$ of 3.6%, demonstrating the significance of fluorescence emission in the SSRC.

Rooftop cooling measurement

We then evaluate the SSRC capacity of our FR coating using a well-insulated apparatus (Figure S5) in Beijing. Detailed descriptions of the cooling performance tests can be found in Supplemental Experimental Procedures S7 and S8. On September 5th and October 3rd, 2018, we measured the cooling effect of the FR coating on an aluminum plate, with the results shown in Figure 3A and B (weather data shown in Figure S6A and B). An obvious sub-ambient cooling effect under direct sunlight is achieved and the respective cooling temperatures are 5±1 and 6±1 °C below the ambient air at the noontime. Such cooling effect is comparable to the best record reported for the existing SDRCs in spite of the lower cost and easier implementation of our FR coating[10,19]. In addition, Figure 3C verifies that our FR coating exhibits an enhanced daytime cooling capability (6±1 °C) yet suppresses nighttime overcooling (4±0.3 °C) on October 4th, 2018, whereas previous SDRC designs usually lead to enhanced nighttime cooling compared to daytime[12,15,16,20,21] (weather data shown in Figure S6C). In building applications, the narrowed diurnal temperature difference can benefit their service life because of the reduced thermal loading[21] and also make our SSRC coating facilitate a more human-comfort temperature. With the measured solar intensity of 744 W/m^2 and temperature reduction of 6 °C on October 5th, 2018 (weather data shown in Figure S6D), the daytime cooling power of our FR coating is measured to be 84.2±8.5 W/m^2 (Figure 3D) with a non-radiative heat coefficient of 4.5 Wm^{-2}K^{-1} as determined with the method described in Supplemental Experimental Procedure S8.5. To eliminate the influence of the substrate on the measured cooling power, the net cooling power was theoretically calculated as 64.5 W/m^{-2} according to the recorded environmental parameters during the testing period (the calculation method is shown in the Supplemental Experimental Procedure S8.6).

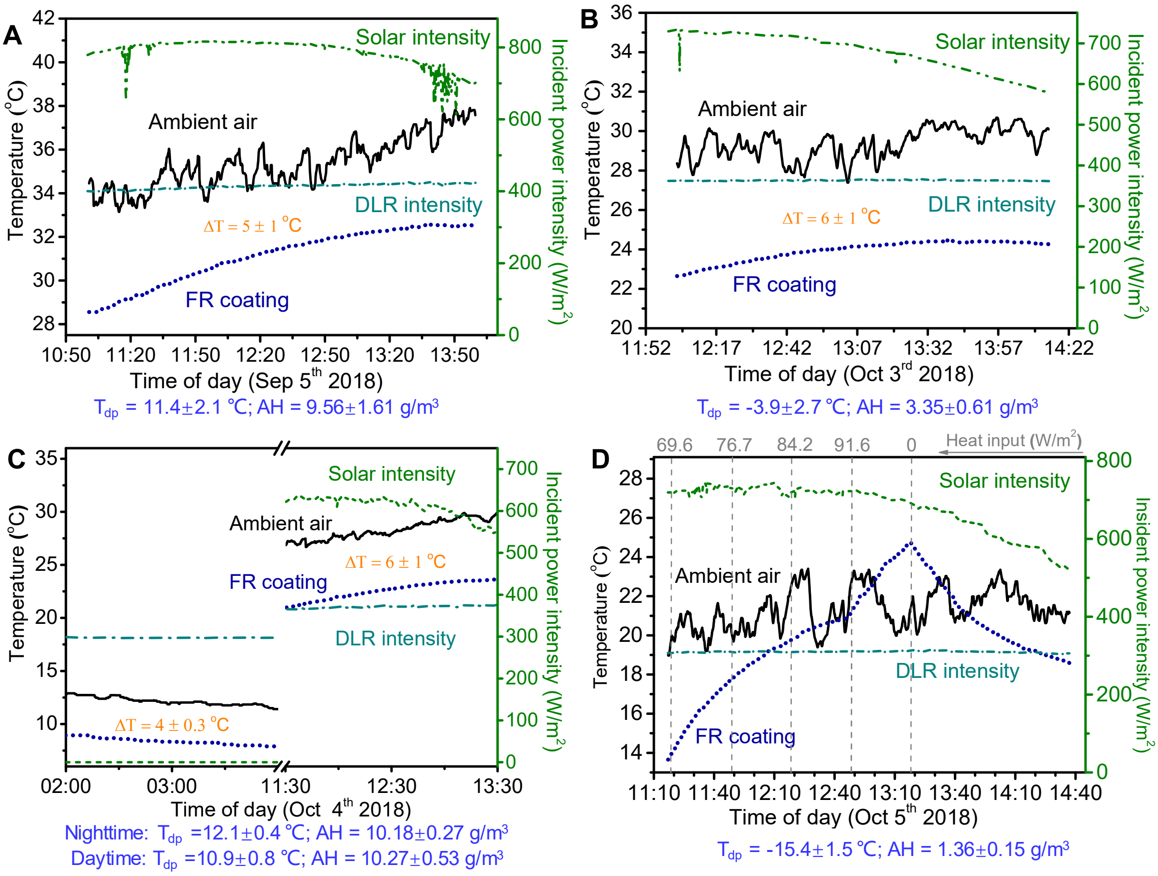

Figure 3. Cooling performance of FR coating over aluminium plate. Measured cooling performance of a painted aluminium plate against the incident solar irradiance and DLR intensity during the noon hours on (A) September 5th, 2018, and (B) October 3rd, 2018 in Beijing. (C) Comparison between cooling temperatures of the FR coating at the noontime and nighttime on October 4th, 2018 in Beijing. (D) Measured FR coating's temperature against the ambient air temperature, in response to the stepped ascending heat input (heat input power shown at top at the beginning of each time period). When the FR coating surface reaches ambient air temperature, the heat input is equal to the net cooling power).

*The T_{dp} and AH values labelled beneath the figures refer to the dew-point temperature and the absolute humidity during the testing period.

To reveal the fluorescence contribution to SSRC, the FR and white coatings are painted, respectively, on two aluminium plates to perform field tests in August, and the result are shown in Figure 4A. During the middy hours of August 23rd, 2018 (weather data shown in Figure S6E), the average temperature of the

FR-coating-painted aluminium plate is approximately 3.3 °C below the ambient air temperature, whereas that coated with the white coating remains slightly above the ambient air temperature. On the one hand, no cooling effect observed for the white coating indicates that the solar absorption by the white coating and its thermal emission to the sky is almost balanced. On the other hand, the significant sub-ambient cooling effect observed for the FR coating clearly reveals the net cooling power contributed by the fluorescence-mediated cooling at the noontime. Even on a cloudy, hazy and windy day (August 27th, 2018, weather data shown in Figure S6F), the two devices remain respectively below and above the ambient air temperature under direct sunlight (inset of Figure 4B). During the night, early morning and late afternoon, their temperatures are nearly superimposed and clearly below the ambient air temperature (Figure 4B), indicating that fluorescent cooling occurs only when the solar intensity is above a certain threshold value. Nevertheless, both sets of results unambiguously illustrate the profound significance of fluorescent emission in the observed SSRC effect.

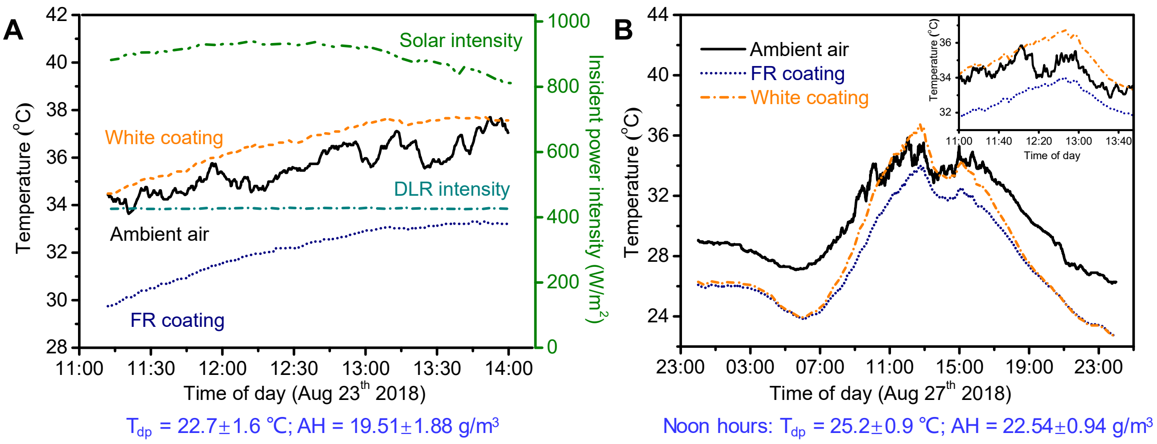

Figure 4. Measured cooling effects of FR and white coatings over aluminium plates. A comparison of the cooling effect between the FR coating and the white coating during **(A)** the midday hours on August 23, 2018 and **(B)** an entire day on August 27, 2018. The inset is an enlargement of the curves during the midday hours.

Cooling performance over scale-model building

For the first time, we carry out a continuous field test on two scale-model buildings (Figure S7A) to clearly elucidate the FR coating's SSRC ability under real working conditions in summer in Beijing, with the results shown in Figure 5. Regardless of the weather conditions (Figure S7B and C), the surface temperature of the painted roof is always below the ambient air temperature over the test period of one week in August in Beijing, with a maximum sub-ambient temperature reduction of 7 °C at the noontime and 1 °C at the nighttime (Figure 5A). Such enlarged sub-ambient daytime cooling yet suppressed nighttime cooling effects in real buildings are probably ascribed to the bulky dimension and substantial thermal mass of the concrete substrate (see Supplemental Text S1). As a result, the diurnal temperature difference of the painted roof surface is even smaller than that of the ambient air (11 °C versus 16 °C). Nevertheless, the coated building's interior temperature is successfully maintained around the human thermal comfort temperature (26 °C), with a sub-ambient temperature reduction temperature reduction ranging from 2°C to 10 °C during the test period (maximum sub-ambient temperature reduction of 9 °C at noontime, Figure 5B).

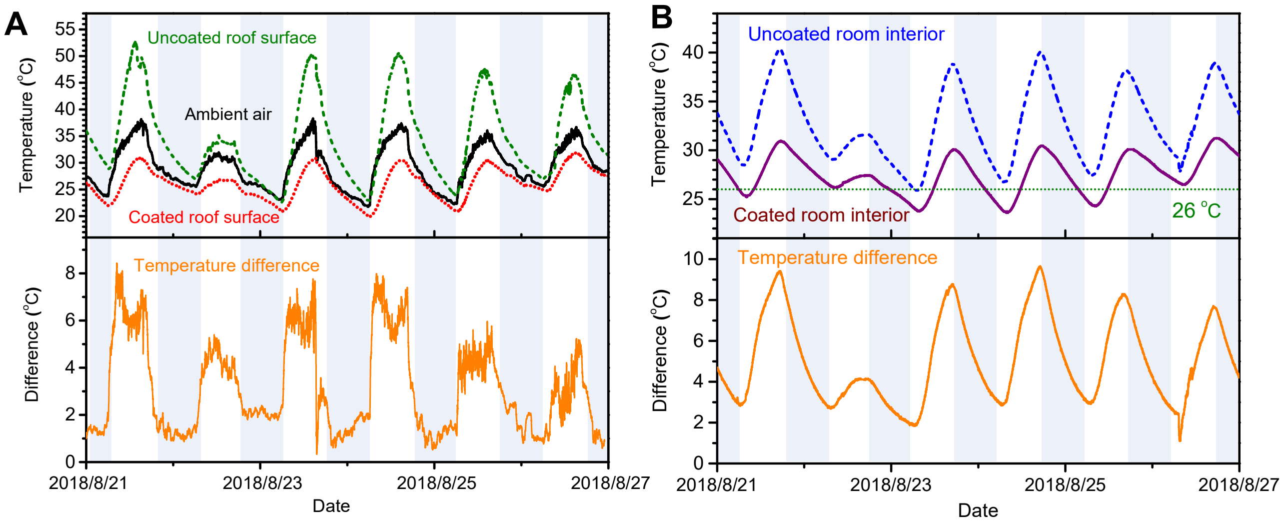

Figure 5. Continuous field tests of the FR coating's cooling effect on scale-model buildings. (A) Top panel: Measured sub-ambient cooling effect of the FR coating painted on the roof surface of a scale-model building against the ambient air temperature from August 21th, 2018 to August 27th, 2018; Bottom panel: calculated temperature difference between the ambient air and the coated roof surface.(B) Top panel: comparison of the room interior temperatures between the coated and uncoated scale-model buildings; Bottom panel: calculated temperature difference between the uncoated and the coated roof interior The shadow parts refer to the nighttime regions (6:00pm-6:00am) and the unshaded parts refer to the daytime regions (6:00 am-6:00 pm).

One important metric that affects the FR coating's SSRC effect is the coating's solar reflectance, which may attenuate over time mainly due to ageing, weathering, and particulate accumulation when exposed to outdoor environments.[32-34] To address this issue, the coating's weather resistance, chemical tolerance and self-cleaning properties are systematically evaluated. After 960 h of artificial accelerated weathering tests, the attenuation ratio of the coating's solar reflectance under the unexcited state is 3.7%. The excellent weather resistance (Figure S8A and Table S2), chemical tolerance (Figure S8B), and the hydrophobic (Figure S8 C-D) self-cleaning (Movie S3) properties jointly enable the FR coating to maintain its high solar reflectivity for a long period, thus ensuring the sustainability of its SSRC effect. Such outstanding long-term durability and environmental applicability of the FR coating not only expands its application scenarios and service lifetimes but also minimizes the maintenance cost of painted building surfaces.

DISCUSSION

The core design of this research is to develop a highly scalable cooling coating material towards the real-world applications of SDRC technologies, especially for large-scale building cooling. The experimental results presented above have clearly demonstrated that a variety of commonly used materials can be employed to fabricate a building coating with a significant SSRC effect. Instead of excessively pursuing the properties of raw materials or relying on sophisticated structural designs, we can also achieve effective cooling performances through simple compensation methods. The designed SSRC coating is not only cost-effective, environmentally friendly and convenient to use in construction, but also shows excellent durability and an outstanding self-cleaning capability. These characteristics remove the practical barriers to the application of current SDRC technologies for large-scale building cooling in real-world conditions.

In conclusion, we have successfully engineered a building coating material with sub-ambient radiative cooling through the combined effects of sunlight-induced fluorescence, particle scattering and materials' broadband emissivity. The proposed broadband radiator makes use of the sky as a temperature regulator to narrow the diurnal temperature difference of our SSRC coating, and also significantly broadens the scope of materials selection. Such generic design concept presented here can also be applied to other surface materials when cooling is in need under the sunlight. The approach presented here is cost-effective and hence opens up a totally new avenue in translating the SDRC technology into broad and practical applications in building environments, reducing the energy demand of building cooling while achieving human thermal comfort, improving human health and productivity.

REFERENCES ANN NOTES

1 Rupp, R. F., Vásquez, N. G. and Lamberts, R. (2015). A review of human thermal comfort in the built environment. *Energy Build.* **105**, 178–205.
2. Hawken, P. (2017). Drawdown: The most comprehensive plan ever proposed to combat global warming.
3. Gentle, A. R. and Smith, G. B. (2010). Radiative heat pumping from the earth using surface phonon resonant nanoparticles. *Nano Lett.* **10,** 373–379.
4. Zhu, L., Raman, A. and Fan. S. (2013). Color-preserving daytime radiative cooling. *Appl. Phy. Lett.* **103**, 223902.
5. Rephaeli, E., Raman, A. P. and Fan, S. (2013). Ultrabroadband photonic structures to achieve high-performance daytime radiative cooling. *Nano Lett.* **13**, 1457–1461.
6. Hossain, M. M., Jia, B. and Gu, M. (2015). A metamaterial emitter for highly efficient radiative cooling. *Adv. Opt. Mater.* **3**, 1047−1051.
7. Lu, X., Xu, P., Wang, H., Yang, T. and Hou. J. (2016). Cooling potential and applications prospects of passive radiative cooling in buildings: The current state-of-the-art. *Renew. Sustain. Energy Rev.* **65**, 1079–1097.
8. Kecebas, M. A., Menguc, M. P., Kosar, A. and Sendur, K. (2017). Passive radiative cooling design with broadband optical thin-film filters. J. Quant. Spectr. Radia. Trans. **198**, 179–186.
9. Huang, Z. and Ruan, X. (2017). Nanoparticle embedded double–layer coating for daytime radiative cooling. *Int. J. Heat Mass Transfer* **104**, 890–896.
10. Raman, A. P., Anoma, M. A., Zhu, L., Rephaeli, E. and Fan, S. (2014). Passive radiative cooling below ambient air temperature under direct sunlight. *Nature* **515**, 540–544.
11. Gentle, A. R. and Smith, G. B. (2015). A subambient open roof surface under the mid-summer sun. *Adv. Sci.* **2**, 1500119.
12. Chen, Z., Zhu, L., Raman, A. and Fan. S. (2016). Radiative cooling to deep sub-freezing temperature through a 24-h day-night cycle. *Nat. Commun.* 7, 13729.
13. Kou, J. L., Jurado, Z., Chen, Z., Fan, S., & Minnich, A. J. (2017). Daytime radiative cooling using near-black infrared emitters. *ACS Photonics*, *4*, 626-630.
14. Chen, Z., Zhu, L., Raman, A. and Fan. S. (2019). Simultaneously and synergistically harvest energy from the sun and outer space. *Joule.* **3**, 101-110.
15. Zhai, Y., Ma, Y., David, S. N., Zhao, D., Lou, R., Tan, G., Yang, R. and Yin. X. (2017). Scalable-manufactured randomized glass-polymer hybrid metamaterial for daytime radiative cooling. *Science* **355**, 1062–1066.
16. Goldstein, E. A., Raman, A. P. and Fan. S. (2017). Sub-ambient non-evaporative fluid cooling with the sky. *Nat. Energy* **2,** 17142**.**
17. Bao, H., Yan, C., Wang, B., Fang, X., Zhao, C. Y. and Ruan, X. (2017). Double-layer nanoparticle-

based coatings for efficient terrestrial radiative cooling. *Sol. Energy Mater. Sol. Cells* **168**, 78–84.

18. Tso, C. Y., Chan, K. C. Chao, C. Y. H. (2017). A field investigation of passive radiative cooling under Hong Kong's climate. *Renew. Energy* **106**, 52–61.
19. Mandal, J., Fu, Y., Overvit, A., Jia, M., Sun, K., Shi, N., Zhou, H., Xiao, X., Yu, N. & Yang, Y. (2018). Hierarchically porous polymer coatings for highly efficient passive daytime radiative cooling. *Science* **362**, 315–319.
20. Zhao, D., Aili, A., Zhai, Y., Lu, J., Kidd, D., Tan, G., Yin. X. and Yang, R. (2019). Subambient cooling of water: Toward real-world applications of daytime radiative cooling. *Joule*, **3**, 111-123.
21. Li, T., Zhai, Y., He, S., Gan, W., Wei, Z., Heidarinejad, M., Dai, J., Chen, C., Aili, A., Vellore, A., Martini, A., Yang, R., Srebric, J., Yin, X. and Hu, L. (2019). A radiative cooling structural material. *Science* **364,** 760-763.
22. Ghali, V., Favre, R. and Elbadry, M. Concrete structures: Stresses and deformations: Analysis and design for serviceability (CRC Press, 2014).
23. Song, Z., Zhang, W., Shi, Y., Song, J., Qu, J., Qin, J., Zhang, T., Li, Y., Zhang, H. and Zhang, R. (2013). Optical properties across the solar spectrum and indoor thermal performance of cool white coatings for building energy efficiency. *Energy Build.* **30**, 49–58.
24. Cool Roof Rating Council, Rated Products Directory. Retrieved from https://coolroofs.org/directory.
25. Santamouris, M. (2014). Cooling the cities – A review of reflective and green roof mitigation technologies to fight heat island and improve comfort in urban environments. *Solar Energy* **103,** 682-703.
26. Berdahl, P., and Bretz, S. E. (1997). Preliminary survey of the solar reflectance of cool roofing materials. *Energy Build.* **25**, 149–158.
27. Levinson, R., Chen, S., Ferrari, C., Berdahl, P. and Slack, J. (2017). Methods and instrumentation to measure the effective solar reflectance of fluorescent cool surfaces. *Energy Build*. **152**, 752–765.
28. Berdahl, P., Chen, S. S., Destaillats, H., Kirchstetter, T. W., Levinson, R. M. and Zalich, M. A. (2016). Fluorescent cooling of objects exposed to sunlight–The ruby example. *Sol. Energy. Mater. Sol. Cells* **157**, 312-317.
29. Jacob, Z.; Smolyaninov, I. I.; Narimanov, E. E. (2012). Broadband Purcell Effect: Radiative Decay Engineering with Metamaterials, *Appl. Phys. Lett*. **100,** 181105−181109.
30. Noda, S., Fujita, M. & Asano, T. (2007). Spontaneous-emission control by photonic crystals and nanocavities (review). *Nature Photonics* **1,** 449–458.
31. ASTM E1918-16: Standard Test Method for Measuring Solar Reflectance of Horizontal and Low-Sloped surfaces in the field.
32. Zhang, W., Song, S., Shi, Y., Song, J., Qu, J., Qin, J., Zhang, T., Li, Y., Xu, L. and Xue, X. (2013). The effects of manufacturing processes and artificial accelerated weathering on the solar reflectance and cooling effect of cool roof coatings. *Sol. Energy Mater. Sol. Cells* **118**, 61–71.
33. Akbari, H., Bretz, S., Kurn, D. M. and Hanford, J. (1997). Peak power and cooling energy savings of high-albedo roofs. *Energy Build.* **25**, 117–126.
34. Akbari, H. and Taha, H. (1992). The impact of trees and white surfaces on residential heating and cooling energy use in four Canadian cities. *Energy* **17**, 141–149.

EXPERIMENTAL PROCEDURE

Full experimental procedures are provided in the Supplemental Information.

SUPPLEMENTAL INFORMATION

Supplemental Information including 10 Supplemental Experimental Procedures, 1 Supplemental Texts, 8 Supplemental Figures, 2 Supplemental Tables, and 3 Supplemental Movies can be found online with this article.

ACKNOWLEDGEMENTS

The authors are grateful for the financial support provided by the National Natural Science Foundation of China (Grant Nos. 51873200; 61535004), the Hong Kong Research Grants Council (GRF Grant No.: 15301414), the Harbin Zhongke Materials Engineering Co., Ltd. (Grant No. BL-2017B-061), the Environmental Conservation Fund of Hong Kong SAR (Project No. K-ZB0D) and the Post-Doctoral Fellowship of the Hong Kong Polytechnic University (Grant No. G-YW2F). The authors are also grateful to Prof. Jianhua Hao and Prof. Harry Atwater for their advice on the interpretation of test results.

AUTHOR CONTRIBUTIONS

W.D.Z. and X.X. conceived the research idea and proposed the overall test program; M.Q. constructed the theoretical model; Y.W.L. and X.X. prepared the materials; Y.W.L., X. X. and M.Q. designed and conducted the optical experiments; Q.M.Z. improved the physical understanding of the problem and provided advice on the research; S.H.F. provided advice on the research particularly relevant to the theoretical part; and Z.Y. and S.Q.L. conducted the experiments relevant to the fluorescence emission. C.F., L.J.X., T.Z., J.Q. and H.Q.W. conducted the cooling effect measurements and verified the constructability; J.-G.D. supervised and supported the research conducted by X.X. and Z.Y.; D.Y.L. and W.J. supervised and supported the research conducted by M.Q. and S.Q.L.; and all authors contributed to the interpretation of test results. D.Y.L. Q.M.Z. J.-G.D. revised the manuscript draft prepared by X.X., M.Q. and W.D.Z.